Electrochimica Acta 519 (2025) 145834

Contents lists available at ScienceDirect

Electrochimica Acta

journal homepage: www.journals.elsevier.com/electrochimica-acta

A point-of-care, label-free OECT sensor for uric acid detection: Validation in human saliva

Francesca Ceccardi [a], Federica Mariani [a,*], Francesco Decataldo [b], Vito Vurro [c], Marta Tessarolo [c], Isacco Gualandi [a], Beatrice Fraboni [c], Erika Scavetta [a]

[a] Department of Industrial Chemistry "Toso Montanari", University of Bologna, Via Piero Gobetti 85, 40129, Bologna, Italy
[b] Department of Medical and Surgical Sciences, University of Bologna, Via Giuseppe Massarenti, 9, 40138, Bologna, Italy
[c] Department of Physics and Astronomy "Augusto Righi", University of Bologna, Viale Berti Pichat 6/2, Bologna, 40127, Italy

ARTICLE INFO

Keywords:
OECT
Electrochemical sensor
PEDOT:PSS
Bioelectronics
Uric acid
Point-of-care
Saliva

ABSTRACT

This study presents the development of an organic electrochemical transistor (OECT) sensor for the detection of uric acid (UA) in human saliva, employing a potentiodynamic measurement technique. Unlike many existing (bio)sensors, this device is entirely based on the organic semiconductor poly(3,4-ethylenedioxythiophene): polystyrene sulfonate (PEDOT:PSS), which simplifies manufacturing and maintenance and reduces production costs. First of all, a systematic comparison between the potentiostatic and potentiodynamic sensing performance in buffer solution is presented, which proves the superior accuracy (14 %), repeatability (5 %), and reproducibility (8 %) of the potentiodynamic approach. In particular, a sensitivity of 59 μS dec^{-1} is obtained in the concentration range 10 – 350 μM UA, with a detection limit of 1 μM. Selectivity studies and subsequent validation of the potentiodynamic OECT sensor in human saliva with an independent method specific for salivary UA quantification is then presented, after which we show the application of our sensor to salivary UA monitoring during food intake, as well as the attempt to analyze swine saliva. Furthermore, as the sensor's design supports integration with point-of-care platforms, we demonstrate its functionality with portable electronics and smartphone connectivity. This approach enables rapid, real-time monitoring, offering a practical and cost-effective solution for non-invasive UA detection in clinical settings.

1. Introduction

The increasing interest in healthcare and the consequent need to monitor people's health conditions are bringing out new point-of-care (POC) technologies, in particular biosensors. POC systems make complex platforms and analyses accessible to a larger number of patients and less specialized types of users, allowing large-scale screening for disease prevention, rapid diagnosis, and better monitoring of treatments [1–3] even where laboratory facilities are not available.

Research focuses on analytes that are representative of the health status and can be collected in a non-invasive way, like the ones contained in sweat, urine, and saliva [4–6].

Uric acid (UA) is a clinically significant analyte due to its role as a major antioxidant and a marker for oxidative stress, which is associated with various health issues such as cancer, cardiovascular, and neurodegenerative diseases [7–15]. As the end product of purine metabolism, UA is normally eliminated from the kidneys through urine in healthy conditions. Elevated UA levels can indicate gout, kidney failure, and cardiovascular diseases, while low levels have been linked to atherosclerosis and stroke [16–24]. The concentration of UA in various biological fluids (such as urine [25], serum [26,27], sweat [28], wound exudate [27], saliva [29,30]) has been quantified in healthy individuals, as summarized in Table S1. Specifically, salivary UA levels have been reported to range from 7.3 to 265 μM [29] and from 40 to 360 μM [30]. Saliva represents a promising biofluid for point-of-care diagnostic applications due to its non-invasive and rapid collection, which makes it particularly suitable for real-time health monitoring. However, its complexity and the micromolar concentration of uric acid require robust, selective technologies. Conventional analytical methods like high-performance liquid chromatography are time-consuming and expensive [25,31]. Consequently, various salivary uric acid sensors, particularly biosensors and electrochemical sensors [32–34] have been developed, though they are often tested in artificial saliva only [35–37]. Electrochemical sensors are advantageous for their short analysis times,

* Corresponding author.
E-mail address: Federica.mariani8@unibo.it (F. Mariani).

https://doi.org/10.1016/j.electacta.2025.145834
Received 20 November 2024; Received in revised form 6 February 2025; Accepted 9 February 2025
Available online 10 February 2025

low cost, and simple procedures [38,39]. Recent advancements in this field include organic electrochemical transistors (OECTs), which operate at low voltages (below 1 V) and feature easy fabrication and unique functionalities. Consisting of three electrodes, e.g., drain, source, and gate, OECTs use a conductive polymer channel such as poly(3, 4-ethylenedioxythiophene):polystyrene sulfonate (PEDOT:PSS) and do not require a reference electrode, allowing for rapid signal acquisition with cost-effective readout electronics [40,41].

In practical applications, OECTs operate in ion-containing fluids, where the drain voltage (Vd) generates the channel current (Id), while the gate voltage (Vg) regulates ion penetration into the channel. This ion flux modulates the doping state of the conductive polymer, affecting the channel's conductivity and, consequently, the drain current [37,42–46]. Thanks to the inherent amplification capability, OECTs are highly sensitive transducers that convert biochemical signals into electronic ones. OECTs work as chemical sensors for redox-active species when the redox reactions involving the analyte, triggered by the proper applied voltage, affect the doping state of PEDOT, resulting in changes to Id proportional to the analyte concentration [47]. Recent studies from our research group have shown that PEDOT-based OECTs are effective sensors for oxidizable molecules like uric acid [48,49], with the transistor configuration providing signal amplification, high sensitivity, low detection limit, and signal filtering [37,50,51].

Among the common sensing strategies for OECTs, potentiostatic and potentiodynamic detections are the most widely used. Potentiostatic measurements involve maintaining fixed drain and gate voltages and recording Id, where the steady-state drain current correlates with the analyte concentration. While simple, this technique can suffer from poor selectivity in label-free, all-PEDOT:PSS OECT sensors, as any analyte undergoing redox reactions at the applied voltages can affect the response [37,51]. On the other hand, potentiodynamic measurements apply a linear potential scan at the gate while maintaining a constant Vd, enabling the differentiation of analytes based on their distinct oxidation potentials. Though more complex, this method facilitates the discrimination of individual analyte contributions and therefore their selective detection [49].

To date, only a few examples of uric acid detection using OECTs have been reported. The first work employed the potentiodynamic technique to distinguish uric acid, ascorbic acid, and dopamine using all-PEDOT OECTs, demonstrating selective detection even with similar oxidation potentials. However, these measurements were conducted in a buffer solution without testing the sensor capability in complex matrices [49]. The following studies [52–54] shifted the detection from buffer solutions to artificial biofluids, such as artificial wound exudate and urine, where background interference led to significant challenges. To improve selectivity, electrode functionalization was introduced, increasing fabrication complexity and costs. Additionally, synthetic biofluids do not provide the full complexity of real matrices. The only example reported to date of UA detection in real saliva involves complex functionalization, achieving a low detection limit, but lacks validation with an independent analytical method [55].

The present study illustrates the development of a novel OECT sensor for the detection of uric acid, exploiting a potentiodynamic transduction mechanism. This sensor is capable of detecting UA in real human saliva without requiring any specific functionalization to address the matrix influence on the measurements. The transistor elements (gate and channel) were entirely fabricated with PEDOT:PSS, offering enhanced biocompatibility and a simplified, cost-effective manufacturing process compared to the aforementioned functionalization approaches.

Our device transduction mechanism is robust and has been validated with an independent analytical method, which is specific for salivary uric acid quantification. Additionally, UA sensing is conducted directly in saliva without advanced sample treatments. Finally, it is worth noting that the device can be easily integrated into POC platforms owing to the rapid measurements enabling in-situ detection, as demonstrated using portable electronics connected to a smartphone via Bluetooth.

2. Experimental

2.1. Chemicals

Uric acid, monobasic potassium phosphate (KH_2PO_4), and potassium hydroxide (KOH) were purchased from Sigma Aldrich. The phosphate buffer solution (PBS) was prepared with 0.1 M KH_2PO_4 and adjusted to pH 7.00 with 1 M KOH. This study involved the use of saliva samples from the authors, with no external participants. As such, no formal ethical approval was sought. Saliva samples used in this study were self-collected by the authors. The authors confirm that the use of these samples complies with institutional and ethical guidelines for self-experimentation. The author declares no conflict of interest related to the use of self-collected saliva samples in this study. Swine saliva samples were sourced from DSM Nutritional Products.

2.2. OECTs fabrication

Glass substrates were cleaned via subsequent sonication in soap (10 % v/v in water), acetone, isopropanol, and distilled water. After the dehydration step (10 min at 110 °C), the Microposit S1818 positive photoresist (from Micro Resist Technology) was spin coated (4000 rpm for 60 s) and annealed at 110 °C for 1 min. Metallic contacts were fabricated using direct laser lithography using the ML3Microwriter (from Durham Magneto Optics). The photoresist was developed with a Microposit MF-319 developer. Then, 7 nm of chromium and 30 nm of gold were deposited by thermal evaporation. Samples were immersed in acetone for 4 h for photoresist liftoff. Metallic contacts were encapsulated using an mr-DWL 5 negative photoresist (from Micro Resist Technology). The resin was spin coated at 3000 rpm for 30 s and annealed at 100 °C for 2 min. After laser exposure, samples were baked at 100 °C for 2 min, relaxed for 1 h at room temperature, and developed using mr-Dev 600 developer (Micro Resist Technology). A final oxygen plasma descum of photoresist residuals (120 W for 4 min) was performed, and then, the negative resist was baked at 120 °C for 30 min. A double layer of S1818 was deposited to pattern the PEDOT:PSS microstructures (OECT channel and gate). After development, substrates were treated with air plasma (15 W for 2 min) to improve polymer adhesion, and the PEDOT:PSS solution (94 % PEDOT:PSS (Heraeus, Clevios PH1000), 5 % of ethylene glycol (EG) (Sigma-Aldrich), 1 % of 3-glycidoxypropyltrimethoxysilane (GOPS), and 0.25 % of 4-dodecylbenzenesulfonic acid (DBSA) was spin coated at 3000 rpm for 10 s. The resulting film thickness was (100 ± 10) nm. The samples were subsequently annealed at 120 °C for 1 h, and S1818 was finally lifted off after 4 h in isopropanol.

2.3. OECTs geometry

A scheme of the device geometry is reported in Fig. 1b. The green areas indicate the presence of an insulating layer (mr-DWL 5 negative photoresist) used for feedlines encapsulation, while the blue ones represent the PEDOT:PSS material of the gate and the channel. The contacts are fabricated with gold. The device is designed with an L-shaped gate, strategically positioned below the channel. This configuration allows the gate to be immersed in a solution without involving the channel. Such a design facilitates the potential use of the gate as a working electrode in an electrochemical cell setup, enabling characterization through techniques like cyclic voltammetry, without direct interaction with the channel. The geometrical parameter γ selected for the microfabrication of the device is 0.33, calculated as $\gamma = \frac{A_g}{A_{ch}}$ where A_g and A_{ch} are the gate and channel areas, respectively. The value was chosen based on previous work of our research group regarding non-functionalized OECT sensors for ascorbic acid [48,49].

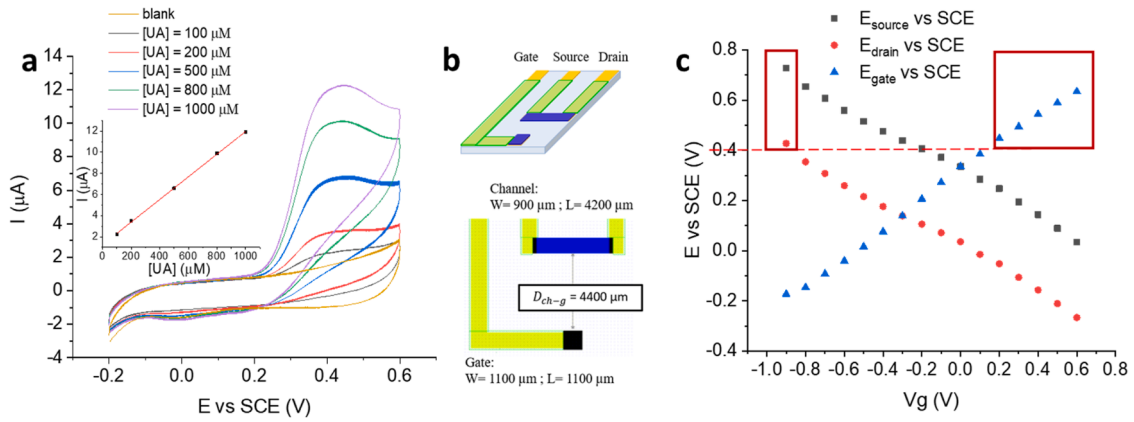

Fig. 1. a) Cyclic voltammograms recorded using a PEDOT:PSS electrode upon incremental additions of UA in 0.1 M PBS, pH 7.00. Scan rate 20 mV/s. Inset: correlation between the oxidation peak current and the analyte concentration. b) Schematic representation of the transistor with channel and gate dimensions. W and L indicate respectively the width (W) and length (L) of the transistor elements, and D_{ch-g} indicates the distance between the channel and the gate. The green areas indicate an insulating layer, the blue ones represent the PEDOT:PSS material of the gate and the channel and the gold areas represent the gold contacts. c) Trend of electrochemical potentials of gate, source, and drain at Vd = −0.3 V as a function of gate voltage in 0.1 M PBS, pH 7.00. The red dotted line highlights the electrochemical potential at which UA oxidation takes place. The red squares identify the Vg windows promoting UA oxidation at the channel/gate.

2.4. Study of OECTs performances

2.4.1. Cyclic voltammetry measurement

The electrochemical responses were recorded employing a CH Instruments 660C potentiostat via cyclic voltammetry with a classical three-electrode cell setup. A PEDOT:PSS film deposited on a gold electrode was exploited as a working electrode and potentials were applied against a saturated calomel reference electrode (SCE) while using a Pt wire as a counter-electrode. The electrodes were immersed in a conventional electrochemical cell containing 0.1 M PBS (pH 7.00) and the current was recorded during the addition of different amounts of uric acid to the electrolyte within an applied potential window ranging from −0.2 V to 0.6 V at 20 mV/s, where PEDOT:PSS is electrochemically stable [56,57].

2.4.2. Electrochemical potentials measurement

The electrochemical potentials of the OECT elements were measured by coupling a Keysight B2902A Source Measure Unit to a CH Instrument 660C potentiostat to carry out simultaneous potential-controlled and open-circuit potential (OCP) measurements. The OECT and a saturated calomel reference electrode were immersed into the electrolyte solution (0.1 M PBS, pH 7.00). The SMU controlled the transistor by applying drain and gate potentials with respect to the source (grounded). In particular, fixed Vd of −0.3 V and Vg from −0.9 to 0.6 V with steps of 100 mV were applied. The potentiostat measured the electrochemical potential of the source (E_{source}) used as a working electrode. Drain and gate electrochemical potentials (E_{drain} and E_{gate}) were calculated by mathematically adding Vd and Vg to E_{source}.

2.4.3. OECTs measurement

The OECT electrical characterizations (output and transfer curves) were carried out in 0.1 M PBS (pH 7.00) using a Keysight B2902A Source Measure Unit (SMU), by applying drain (Vd) and gate (Vg) voltages and measuring the drain (Id) and gate (Ig) currents. Potentiostatic measurements were carried out maintaining fixed Vd of −0.3 V and Vg of +0.6 V and recording Id while adding different amounts of uric acid to 0.1 M PBS (pH 7.00) under magnetic stirring in a concentration range between 5 and 500 µM. The steady-state drain current is the analytical signal that correlates with the analyte concentration. The parameter t_{90} is used to evaluate the response time and indicates how much time is required to reach 90 % of the final signal, which is the steady state current recorded after the addition of uric acid concentration.

Potentiodynamic measurements were carried out maintaining a constant Vd of −0.3 V while applying a linear scan of potential at the gate between −0.5 and 0.6 V with a scan rate of 10 mV/s. The resulting Id vs Vg curve, which sweeps from negative to positive potentials and returns to the initial value, consists of 2 scans, e.g., one measurement cycle. This process can be repeated multiple times to obtain subsequent cycles (second, third, etc.) and assess any variations among them. Id vs Vg curves were recorded while adding different amounts of uric acid to 0.1 M PBS (pH 7.00) in a concentration range between 10 and 500 µM. The transconductance (gm) curves were obtained as derivatives of the experimental curves and gm peak intensity is the analytical signal that correlates with the analyte concentration. A complete comparison between potentiostatic and potentiodynamic is presented in terms of sensitivity, limit of detection (LOD), precision, accuracy, repeatability, and reproducibility. The sensitivity of the measurement was estimated by the slope of the calibration curve. LOD values were calculated using the 3σ/m criterion (where σ is the standard deviation of the blank and m is the slope of the calibration curve), according to [39]. The repeatability and reproducibility were assessed by calibrating respectively the same sensor three times or three different sensors, and considering the relative standard deviation (RSD) among the slopes of the correspondent curves. To evaluate the accuracy and precision, solutions with known concentrations included in the linear range of response were analyzed five times with pre-calibrated sensors, and the recorded analytical signal was used to estimate the analyte concentration from the calibration curve. Accuracy was quantified as the percentage error (% error), determined as variability among the concentrations obtained from the five independent measurements and the known concentration value. Precision was evaluated as the standard deviation relative to the mean concentration obtained from the five measurements.

2.4.4. Saliva samples preparation

Human saliva samples were diluted with 0.1 M PBS pH 7.00 according to the dilution factor. For a 1:2 ratio, 1 mL of PBS was mixed with 1 mL of saliva. For 1:16 ratio, 1 mL of saliva was mixed with 15 mL of PBS. For a 1:21 ratio, 1 mL of saliva PBS was mixed with 20 mL of PBS.

2.4.5. Validation of the measurement

To validate the system for uric acid detection in saliva, the comparison with an independent analytical method was carried out. In particular, the commercial colorimetric kit from Salimetrics was used (Salivary uric acid assay kit #1–3802). The protocol requires several steps like saliva sample pretreatment with vortex and centrifuge, the heating of the kit reagents at 37 °C, a microplate incubator/shaker

operating at 37 °C, and a plate reading with a wavelength of 515 mm.

2.4.6. Measurements with portable electronics

To demonstrate the possibility of using the system for in situ applications, the developed sensor was equipped with wireless and portable custom-made electronics powered by a coin cell battery provided by Elements Srl. It contains a Bluetooth module, which allows wireless control and data transmission to a smartphone via a dedicated application.

3. Results and discussion

3.1. Electrochemical and electrical characterization

Preliminary electrochemical characterizations were performed with uric acid to study its oxidation reaction. In particular, Cyclic voltammetry (CV) experiments were conducted to investigate the electrochemical behavior of a PEDOT:PSS working electrode (i.e., the gate electrode of the OECT structure) in a buffer solution containing different amounts of UA (Fig. 1a). The cyclic voltammograms, recorded within the potential window where PEDOT:PSS is electrochemically stable [56, 57], show a redox wave, whose peak current depends on the UA concentration. It is ascribable to UA oxidation, as UA ($C_5H_4N_4O_3$) can undergo irreversible oxidation at a PEDOT:PSS electrode, following the reaction [58]:

$$C_5H_4N_4O_3 + 2H_2O \rightarrow C_4H_6N_4O_3 + CO_2 + 2H^+ + 2e^-$$

The reaction leads to the formation of the oxidation product allantoin ($C_4H_6N_4O_3$), carbon dioxide, hydrogen ions, and two electrons. The voltammograms, which exhibit a lack of significant reduction peaks, confirm the irreversibility of this oxidation reaction.

The oxidation potential of UA was found to start at approximately 0.25 V vs SCE, with an observed peak maximum at 0.40 V. As evident from the correlation between the current intensity of the corresponding oxidation peak and the analyte concentration (shown in the inset of Fig. 1a), the electrode effectively functions as a transducer to convert the chemical signal associated with uric acid into an electrical signal. Therefore, it can be embedded in an OECT architecture to design a sensor for UA detection with a simple structure as reported in Fig. 1b. In particular, a thin layer of PEDOT:PSS was deposited between source and drain onto a glass substrate to form the channel as well as the gate of the device. The electrical characterizations of the OECT, specifically output and transfer curves, are illustrated in Figure S1a and Figure S1b, respectively. These characterizations can be explained through the electrochemical processes occurring within the OECT system, driven by the variation of the gate voltage, in accordance with the doping−dedoping mechanism involving PEDOT:PSS [59]:

$$GATE: PEDOT^0 + K^+PSS^- \rightarrow PEDOT{:}PSS + K^+ + e^-$$

$$CHANNEL: PEDOT{:}PSS + K^+ + e^- \rightarrow PEDOT^0 + K^+PSS^-$$

where K^+ stands for cations in the electrolyte solution (PBS). A positive Vg leads to a positive polarization of the gate electrode, which induces the oxidation of the polymer. The resulting electrons removed are then injected into the channel, thereby reducing the amount of charge carriers delocalized in the PEDOT:PSS. Consequently, an increase in Vg results in a decrease in the channel's electrical conductivity, which is directly proportional to the concentration of electron holes. This change is transduced in a decrease of Id and the opposite process occurs with negative Vg. This phenomenon is evident in the output curves (Figure S1a), where a stepwise increase in Vg induces a progressive decrease in Id across the recorded curves, as well as in the transfer curves (Figure S1b), where the current value decreases with increasing gate voltage.

The drain and gate voltages required for efficient UA oxidation were determined (Fig. 1c) through the evaluation of the electrochemical potentials (E) of the OECT elements.

When one transistor element exceeds the uric acid oxidation peak potential of 0.40 V, the reaction occurs at either the gate or the channel, depending on the applied potentials. Specifically, the application of a Vd of −0.3 V and a more negative Vg of −0.9 V (initial measurement condition) facilitates the oxidation of uric acid at the channel, thanks to the higher E measured at the channel. In contrast, a positive Vg promotes oxidation at the gate. Summarizing, as it is evident from Fig. 1c, uric acid oxidation takes place at the channel with a Vg lower than −0.9 V, or at the gate with Vg higher than 0.2 V (considering Vd = −0.3 V).

3.2. Uric acid sensing in buffer solution

To avoid extremely negative gate potentials and to achieve optimal oxidizing conditions within the stability window of PEDOT, the option where the oxidation of uric acid occurs at the gate electrode was selected. Consequently, the transduction mechanism relies on the aforementioned electrochemical oxidation of UA at the gate, producing allantoin, carbon dioxide, hydrogen ions, and two electrons [58]. In an all-PEDOT OECT, these electrons are subsequently injected into the channel, resulting in the reduction of the polymer in the film according to the reactions described here [58]:

$$GATE: C_5H_4N_4O_3 + 2H_2O \rightarrow C_4H_6N_4O_3 + CO_2 + 2H^+ + 2e^-$$

$$CHANNEL: PEDOT{:}PSS + K^+ + e^- \rightarrow PEDOT^0 + K^+PSS^-$$

According to the electrical characterization related to the doping-dedoping mechanism of PEDOT, this reduction alters channel electrical conductivity and decreases the drain current. This current modulation, which was also observed in PBS, is boosted by the faradaic contribution from the redox reaction involving uric acid and PEDOT [49,59].

Both potentiostatic and potentiodynamic techniques were employed for UA sensing in aqueous buffer solutions. In potentiostatic measurements, a stepwise decrease in drain current (Id) was observed upon incremental additions of UA (from 5 to 500 μM) to the electrolyte under stirring (Fig. 2a). This behavior is attributed to the progressive reduction of PEDOT:PSS and conductivity of the channel according to the increasing faradic contribution due to UA oxidation on the gate. These potentiostatic measurements led to a linear calibration curve correlating the steady-state Id with the logarithm of UA concentration (Fig. 2b) with a slope of 27 μA/dec for the measurement shown below. The blank current, recorded in PBS before any additions of the analyte, was subtracted to Id to highlight the variations induced by the addition of the analyte. The investigated range of concentration includes the one of interest in saliva found in the literature (40–360 μM) [30]. Furthermore, the sensor has a fast response time (t_{90} = 48 s, defined in the Experimental section) and the use of Id instead of Ig (shown in the inset of Fig. 2a) as an analytical signal provides noise filtering and signal amplification [60].

Potentiodynamic measurements were conducted by recording the Id as a function of Vg and are presented in the supporting information (Figure S2). These curves demonstrate an increasing modulation of Id with higher UA concentrations. The analytical signal in the potentiodynamic approach is the transconductance (gm), defined as a $gm = \Delta Id/\Delta Vg$, where ΔId and ΔVg represent Id and Vg variations, respectively, recorded during the acquisition of transfer curves. Typically, gm exhibits a peak at the Vg where maximum Id modulation is achieved due to the faradaic processes occurring at the gate. Fig. 2c shows the increase in the gm peak upon increasing additions of UA and the resulting calibration plot, reporting a linear correlation between the gm peak and the logarithm of UA concentration (Fig. 2d) between 10 and 350 μM, which is again consistent with the concentration range of interest for the analysis of saliva but slightly more limited compared to potentiostatic measurement. Moreover, differences between the quality

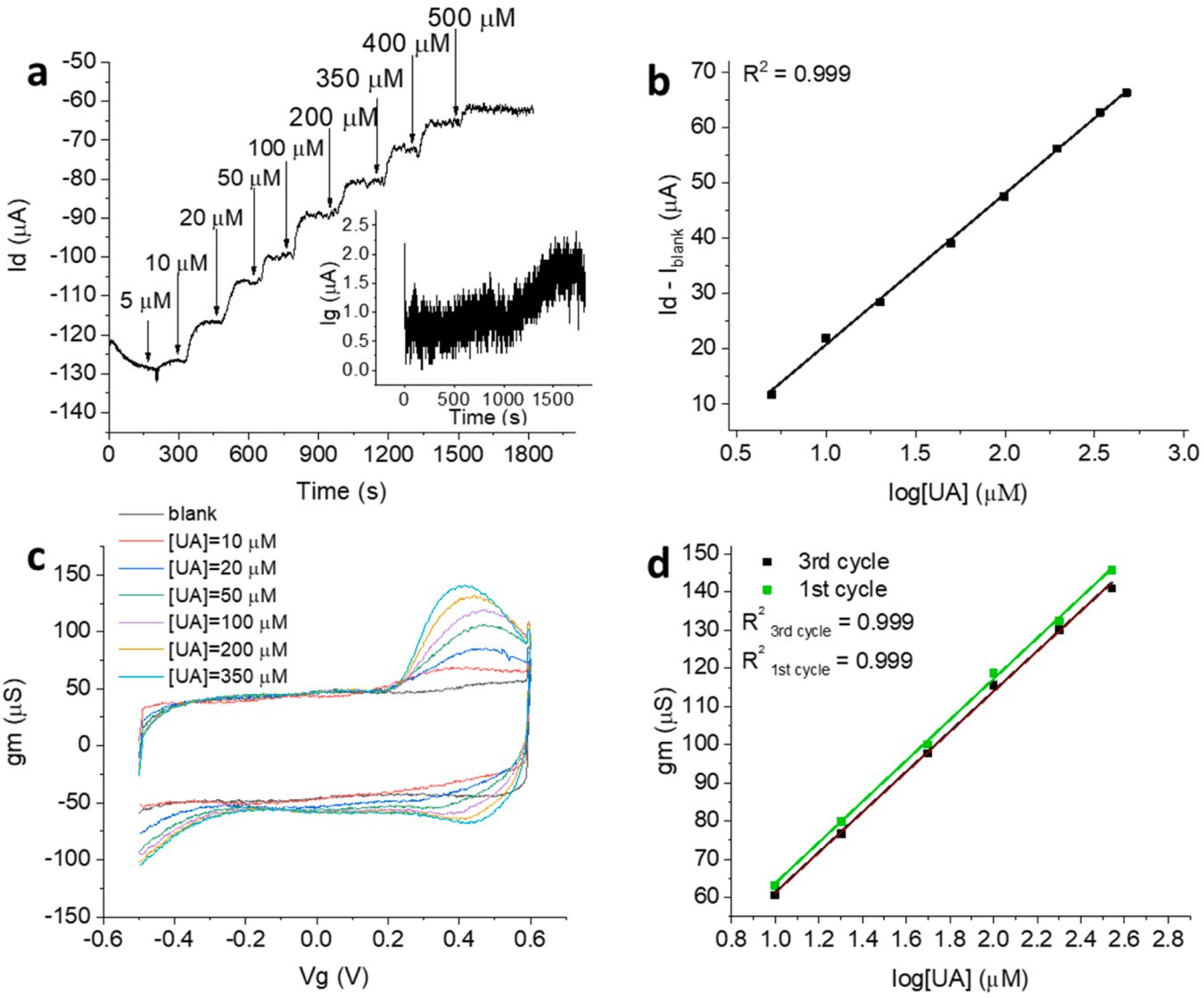

Fig. 2. a) Id vs time curves recorded for incremental additions of UA from 5 to 500 μM to PBS (0.1 M, pH 7.00). Vg = +0.6 V; Vd = −0.3 V. Inset: Corresponding Ig vs time curve. b) Calibration curve obtained from the graph in Fig. 2a. c) gm vs Vg curve recorded for incremental additions of UA from 10 to 350 μM to PBS (0.1 M, pH 7.00). Vg from −0.5 to +0.6 V; Vd = −0.3 V. d) Calibration curve obtained from the graph in Fig. 2c.

of the calibration obtained using the first or the third cycle of Vg sweep were evaluated (Table S2) obtaining slopes of 54 and 53 μS/dec, respectively. Since the values are statistically equivalent, the 1° cycle was chosen for further investigations, as it guarantees a significant decrease in the calibration time without lowering the sensor performance.

A complete comparison between the two sensing strategies (e.g., potentiostatic and potentiodynamic) is presented in terms of sensitivity, limit of detection (LOD), precision, accuracy, repeatability, and reproducibility in Table 1, as described in the Experimental section. The curves related to repeatability and reproducibility are reported in the supporting information for both potentiostatic (Fig. S3) and dynamic (Fig. S4) methods. The analyses of solutions with two known concentrations included in the linearity range of response, e.g., 35 μM for potentiostatic and 100 μM for potentiodynamic, which were employed to assess accuracy and precision, are also included in the supporting information (Fig. S3c and Fig. S4c respectively). Figure S3c illustrates how the potentiostatic results are evenly distributed around the corresponding points on the calibration curve, indicating excellent precision but lower accuracy compared to the actual concentration value. Conversely, the potentiodynamic data reported in Fig. S4c exhibit a less precise distribution of values but higher accuracy compared to the true value.

Table 1
Comparison of the sensors' performances in buffer solution (0.1 M PBS pH 7.00) using potentiostatic and dynamic modes.

	Potentiostatic detection	Potentiodynamic detection
Sensitivity ± SD	(31 ± 4) μA dec^{-1}(*N* = 3)	(59 ± 1) μS dec^{-1}(*N* = 3)
LOD (μM)	3	1
Precision (%RSD) in [UA] estimation	4 % (*N* = 5)	10 % (*N* = 5)
%Error in [UA] estimation	27 % (*N* = 5)	14 % (*N* = 5)
Repeatability	10 % (*N* = 3)	5 % (*N* = 3)
Reproducibility	12 % (*N* = 3)	8 % (*N* = 3)

While potentiostatic measurements are rapid and simpler, the potentiodynamic detection exhibits enhanced sensitivity and a lower LOD, making it particularly suitable for applications requiring reliable quantification of UA. In addition, the accuracy, repeatability, and reproducibility of the potentiodynamic method surpass those of the

potentiostatic detection, although the latter exhibits slightly superior precision. Overall, the potentiodynamic approach was considered more suitable for uric acid detection due to the aforementioned performance advantages and was selected for further investigations. The superior analytical performance achievable with the potentiodynamic method can be explained by considering that, in a device without the reference electrode, the application of a potential scan instead of a fixed potential value ensures higher robustness, mitigating possible variation in the applied voltages.

3.3. Uric acid sensing in saliva

3.3.1. Selectivity measurements

Once the analytical technique was optimized, preliminary tests on the sensor selectivity over interference compounds were carried out. Based on the composition of human saliva reported in the literature [61], different classes of compounds were evaluated and selectivity over lysozyme (as representative for the class of enzymes), cortisol (for hormones), glucose (for sugars) and lactate (for bio-produced organic acids) was tested. Moreover, since all-PEDOT:PSS OECTs have already been employed not only for uric acid, but also for the detection of other oxidizable molecules like ascorbic acid and dopamine [49], these compounds were also tested. To investigate the sensor response in the presence of the interference compounds, an average concentration of the specific analytes was chosen based on the salivary ranges reported in literature. Specifically, 100 μM UA [29,30], 0.48 μM lysozyme [62], 0.2 mM lactate [63], 55.5 μM glucose [64], 20 nM cortisol [65], 5 μM ascorbic acid [66], and 0.5 nM dopamine [67]. To ensure proper system response, blank measurements (in 0.1 M PBS, pH 7.00) were recorded before and after each test with the interfering compounds (only one blank curve is reported here for graphical reasons). Fig. 3a shows the response to the three antioxidants, while Fig. 3b illustrates the response to other characteristic molecules in saliva. No significant sensor response was observed in the potential range of interest at the concentration level found in saliva for any of the interference compounds tested, which closely matched the blank curve.

3.3.2. Evaluation of matrix effect in human saliva and validation with an independent analytical method

Once the selectivity tests were carried out, a calibrated sensor was tested in untreated human saliva (Fig. 4a), showing the capability of the device to work in a real biological medium. Further measurements in human saliva were carried out, in particular recovery tests (Fig. 4b). Specifically, the addition of the analyte to saliva was expected to proportionally increase the analytical signal in accordance with its concentration, starting from the lowest gm value for pure saliva. Instead, pure saliva exhibited the highest transconductance, and the addition of uric acid caused a decrease in the response. This behavior suggested the presence of a matrix effect, which may influence the accuracy of UA detection. It is worth mentioning that the lack of a supporting electrolyte in the real sample is also likely to affect the sensor response, when compared with measurements carried out in PBS. To address these issues, a screening of dilution conditions for saliva samples was performed to optimize accuracy. The optimal dilution factor was selected by comparing the OECT results with an independent analytical method, employed to validate our potentiodynamic approach. In particular, a commercial color assay kit specific for salivary uric acid was chosen for sensor validation, requiring a multistep protocol for sample treatment and analysis, for which laboratory facilities are needed. The comparison of OECT results with the independent method is reported in Table 2, indicating the dilution factor of 1:21 as the most effective to minimize the impact of the matrix while preserving the sensor ability to determine UA. This enabled reliable detection of UA in real saliva samples as evidenced by transconductance curves (Fig. 5a), calibration curves (Fig. 5b), and recovery tests (Fig. 5c), which demonstrate the proper correlation of the signal with concentration. Moreover, stability tests were carried out to demonstrate sensor robustness for 50 repeated measurements in saliva carried out on the same day using the same sensor (Fig. S5). The resulting transconductance is (95 ± 2) μS, with a small relative standard deviation (about 2 %) that highlights the excellent durability of our sensor upon repeated use in human saliva.

The stability of the calibration over time and the re-usability of the sensors after repeated measurements were also investigated. Five calibrations in total were performed with the same OECT sensor during a 17 days long period (Figure S6) and we report the full procedure as well as calibration parameters in Table S3. Overall, considering the sensitivity values, the OECT sensor response was proven to be stable upon repeated use in buffer and saliva samples for >2 weeks. Some shift in the intercept value is also evident from the curves and this change is likely due to aging. However, a simple 2-point calibration procedure, as carried out in the last two cases, still allows the user to reliably carry out quantitative determinations.

3.3.3. Variation of uric acid concentration in human saliva during food intake

After validation, our method was employed to investigate the dynamic changes in salivary UA concentration according to diet and revealed notable fluctuations. In particular, UA increases in patients

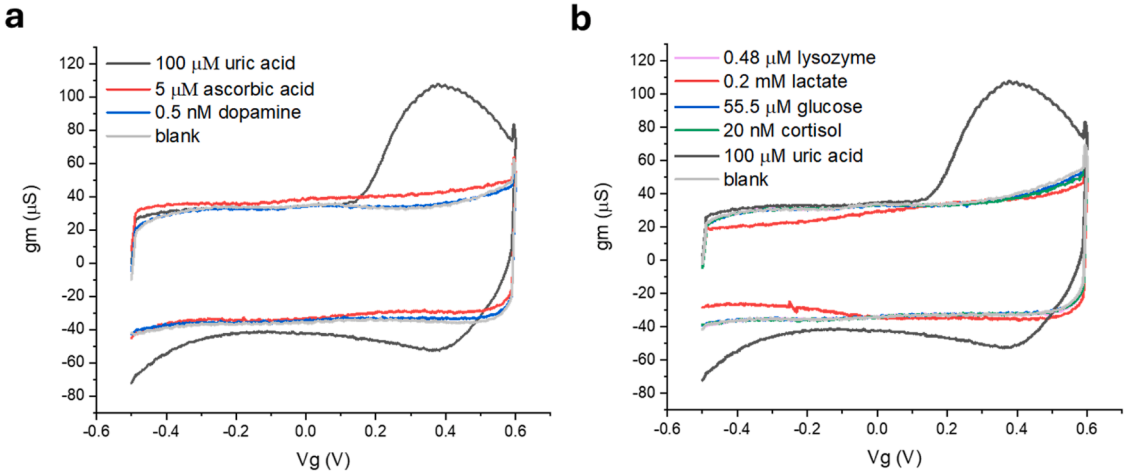

Fig. 3. a) gm vs Vg curves recorded in the presence of uric acid, ascorbic acid, and dopamine in PBS (0.1 M, pH 7.00) to study the sensor response to the three antioxidants considering their typical concentration in human saliva. b) gm vs Vg curves recorded in the presence of lysozyme, lactate, glucose, cortisol, and uric acid to PBS (0.1 M, pH 7.00) considering their typical concentration in human saliva. Scan rate: 10 mV/s.

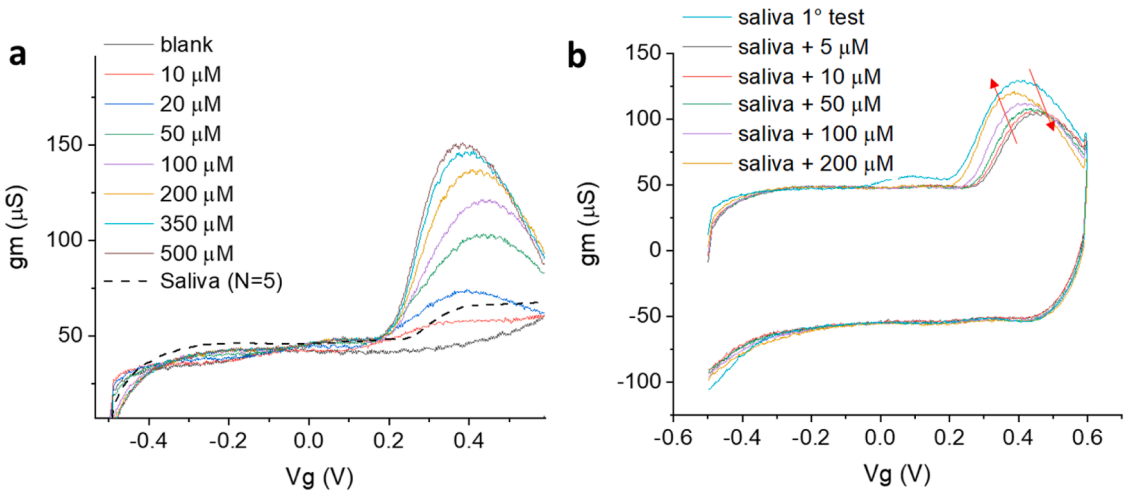

Fig. 4. a) gm vs Vg curves recorded in human saliva (dotted line) compared to the curves recorded during calibration, with UA ranging from 10 to 500 μM in buffer solution. b) Recovery test carried out for incremental additions of UA to pure saliva, with red arrows indicating the unexpected trend of transconductance linked to the presence of a matrix effect.

Table 2
Comparison between UA concentration in human saliva estimated by an independent analytical method (commercial kit) and by OECT sensors with different dilution factors. The error is calculated as standard deviation.

	Mean kit [UA] (μM)	[UA] in pure saliva (μM)	[UA] in saliva 1:16 (μM)	[UA] in saliva 1:21 (μM)
Human saliva 1	332 ± 11	57 ± 26	192 ± 2	336 ± 8
Human saliva 2	358 ± 12	72 ± 5	203 ± 24	342 ± 8
Human saliva 3	344 ± 25	59 ± 4	231 ± 6	376 ± 9

with a high protein diet and with dental caries, and is associated with oxidative stress [68,69]. Saliva samples collected on an empty stomach exhibited a specific baseline UA concentration (222 ± 7) μM for three samples of 1:21 diluted saliva, which increased significantly after food consumption (250 μM) and gradually returned to baseline levels after digestion (218 μM). This fluctuation can indicate an inflammation phenomenon associated with eating. These findings underscore the potential utility of the developed sensor for monitoring physiological responses to dietary habits and health status.

3.3.4. *Uric acid sensing in swine saliva*

In recent years, the use of saliva for biomarker determination has garnered significant interest due to its non-invasive collection process, which is particularly advantageous in animals like swines, where blood sampling induces considerable stress [70,71]. The continuous production of free radicals and other oxidants as by-products of the respiratory chain requires a robust antioxidant defense system to prevent cellular damage [72]. Among these antioxidants, uric acid is a critical biomarker due to its predominant role in neutralizing oxidative stress. Consequently, we explored the possibility to apply the OECT sensor validated in human saliva to the analysis of swine saliva. Concentrations estimated with the OECT sensor and with the commercial kit employed for the former measurements are listed in Table 3. Compared to the experiments in human saliva, the accordance between the two methods is worse. This is likely due to the concentration of uric acid in swine saliva, which has

Table 3
Comparison between UA concentration in swine saliva estimated by OECTs and by an independent method.

	[UA] OECT (μM)	[UA] kit (μM)
Swine saliva 1	35	42
Swine saliva 2	26	23
Swine saliva 3	47	22

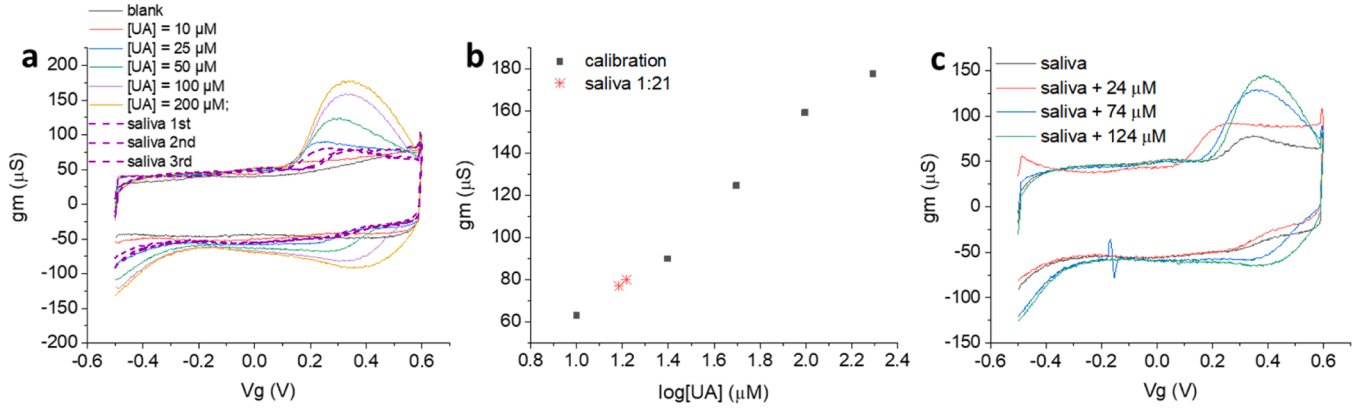

Fig. 5. a) gm vs Vg curves recorded in human saliva diluted with a 1:21 ratio (dotted lines) compared to curves obtained for incremental additions of UA from 10 to 200 μM in buffer solution. b) Corresponding calibration curve including the gm values obtained from the potentiodynamic analysis of diluted saliva. c) Recovery test carried out for incremental additions of UA to diluted saliva showing the absence of a matrix effect.

been reported to be lower than the human one (5–98 μM) [13] and, keeping this in mind, it is worth pointing out that (i) the commercial kit is specific for human saliva and the certified LOD and LOQ (limit of quantification) of 11 and 20 μM, respectively, fall inside the expected concentration range, while, thanks to the lower LOD, our OECT sensor might still guarantee accurate measurements; (ii) due to the lower expected UA concentration, the swine saliva samples were not diluted, which might contribute to the reduced accordance of the results. Due to the absence of standard analytical methods for UA quantification in swine saliva, these tests cannot be properly validated, but still demonstrate once more the robustness of the potentiodynamic OECT sensor, which can successfully assess UA concentration in real biological samples, with potential applicability to non-invasive, in-situ analyses.

3.3.5. *Integration with portable electronics*

It is worth pointing out that the low applied voltages (<1 V) and the compactness of the device make it compatible with the use of a portable electronic readout, which is a must in view of POC applications. The application of the OECT as a portable sensor requires preferentially the investigation of small amounts of saliva, in the order of microliter volumes. Therefore, tests with a transistor equipped with a well containing 250 μL of saliva sample (Fig. S7) were carried out to demonstrate the applicability to small volumes. This sensor was then equipped with a coin cell battery-sized portable electronics prototype containing a Bluetooth module, which allows wireless control and data transmission to a smartphone via a dedicated application. As a proof of concept, a potentiostatic measurement was carried out in PBS recording the decrease of the Id absolute value upon uric acid addition. The response obtained in PBS before (Fig. 6a) and after the addition of 20 μM uric acid (Fig. 6b) is reported in Fig. 6 showing the expected trend. This demonstrates the possibility of using this system for in situ applications with cheaper and simpler equipment than bulky lab-scale setups.

3.4. *State of the art: OECTs for uric acid detection*

Very few examples of UA detection by OECTs have been described in the literature and are listed in Table 4. In the first work, our research group employed the potentiodynamic technique to successfully distinguish uric acid, ascorbic acid, and dopamine with all-PEDOT:PSS OECTs [49]. This paper demonstrates selective detection even when analytes present close oxidation potentials, envisioning the all-PEDOT:PSS OECT as bioanalytical sensor for real-life applications. However, all measurements were carried out in a buffer solution without investigating the capability of the sensor to work in a complex matrix. Following studies [52–54] shifted the detection from buffer solutions to artificial biofluids. In the first manuscript, *Galliani* et al. investigated the detection of uric acid with flexible OECTs in artificial wound exudate. The system requires an enzyme-based hydrogel cast onto a carbon gate and a channel of PEDOT:PSS [52]. In another work, *Tao* et al. presented the fabrication of a device with a PEDOT/carbon fibers gate modified with a molecularly imprinted polymer (MIP) membrane. In particular, a PEDOT nanocluster structure was synthesized on graphene oxide (rGO) modified cotton fibers and the MIP was deposited on this surface. The sensor was exploited to detect uric acid in artificial urine samples [53]. In the third work, *Hao* et al. carried out the detection thanks to a MIP-based OECT to selectively monitor adrenaline and uric acid in artificial urine samples. The PEDOT:PSS gate was functionalized with multi-walled carbon nanotubes (MWCNTs) [54]. Our research group recently described a smart bandaid integrated with a fully textile OECT for uric acid real-time monitoring in artificial wound exudate [59]. It shows a novel application of a textile and label-free sensor, but the detection was only demonstrated in a synthetic medium. The only example in the literature of uric acid detection in saliva is the work by Liao et al., which employs a complex bio-functionalized transducer (uricase(UOx)-glutaraldehyde/Polyaniline(PANI)/Nafion-graphene/Platinum(Pt)). This approach achieves an impressively low detection limit of 3.0 nM. However, the detection in saliva has not been validated with an independent analytical method [55].

The next crucial step towards achieving the technological maturity required for commercialization is the validation of the sensor with an independent method. The aim is to assess and quantify any potential interference from chemical compounds present in the sample matrix, which could impact the accuracy of the uric acid determination. The results presented here represent the first example of a validated OECT sensor for salivary uric acid detection, clearly demonstrating the reliability and robustness of the proposed approach. To further advance the technological readiness of these devices, their performance must be rigorously tested across a statistically significant number of samples to provide a more comprehensive evaluation of the sensor's reliability and consistency, which is essential for real-world applications and eventual commercialization.

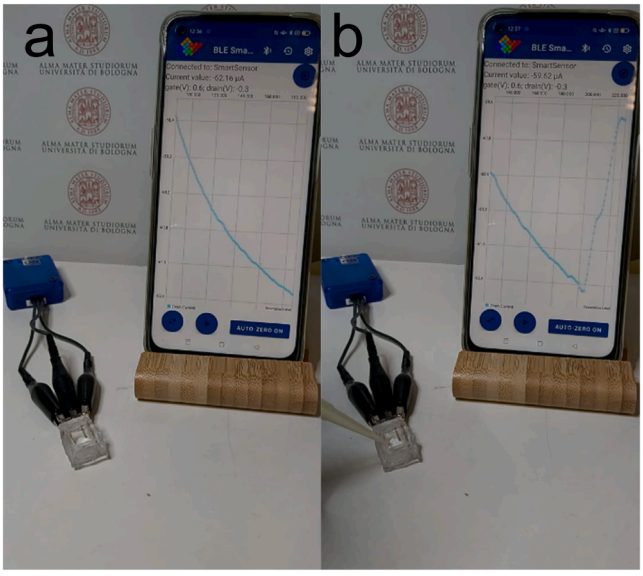

Fig. 6. Id vs time curve recorded with portable electronics before (a) and after (b) the addition of UA.

4. Conclusions

This study presents a novel PEDOT:PSS sensor for detecting salivary uric acid, designed to overcome major limitations in the field. Traditional UA detection methods often face interference from complex biological matrices and require laborious sample preparation, which make them unpractical for real-world use and POC applications. Our OECT-based sensor uses a robust electroanalytical technique and it solely requires an optimized sample dilution to perform quantitative detection in human saliva. A key innovation is the elimination of additional functionalizations, simplifying production, maintenance and reducing costs, while the exclusive use of biocompatible PEDOT:PSS ensures suitability for biological applications. The sensing strategy was defined starting from the analytical study of the transduction mechanism, and then systematically optimized to enhance robustness and sensitivity, contextually exploring the two main sensing approaches in the OECT field. Differently from many other literature examples, the final use of the sensor in the biofluid of interest was not limited to a proof-of-concept study. Extensive characterization of its selectivity and stability led to the final validation through an independent analytical method specific to salivary UA quantification. Following validation, we demonstrated salivary UA monitoring during food intake and challenged our sensor versatility by analyzing swine saliva samples. Overall, the sensor's design and rapid response facilitate easy integration into point-of-care platforms, as also shown by its compatibility with portable electronics.

Table 4
Comparison among the performance of OECTs for uric acid detection.

Functionalization	Sensitivity	Response range	LOD in PBS	Sample	Analysis in real samples	Recovery tests	Validation with independent methods	Reference
None	0.4 S M^{-1}	40 μM – 0.4 mM	20 μM	PBS	no	no	no	[49]
Enzyme-based hydrogel cast onto carbon	N/A	10 μM –1.0 mM	10 μM	artificial wound exudate	no	no	no	[52]
PEDOT/carbon fibers gate modified with a MIP	0.1 mA dec^{-1}	1 nM – 0.5 mM	1 0.0 nM	artificial urine samples	no	yes	no	[53]
MIP/MWCNTs	$3.0{\cdot}10^{-3}$ NCR dec^{-1}	1.0 pM – 1.0 mM	1.0 pM	artificial urine samples	no	yes	no	[54]
None	0.4 dec^{-1}	0.1–1.1 mM	75 μM	artificial wound exudate	no	no	no	[59]
None	59 μS dec^{-1}	10 μM – 0.3 mM	1.0 μM	human and swine saliva	yes	yes	yes	This work
UOx-glutaraldehyde/PANI/ Nafion-graphene/Pt	0.1 V dec^{-1}	10 nM - 30 μM	3.0 nM	human saliva	yes	no	no	[55]

N/A: not available. NCR: normalized current response, here used to compare the sensor performance under different Vg. The formula NCR = $(I_{analyte} - I_0)/I_0 \times 100$ was used, where I_0 and $I_{analyte}$ are the steady-state drain currents recorded before and after adding the analyte, respectively.

These combined innovations mark our device as a significant advancement in salivary UA monitoring, merging advanced detection capabilities with practical application potential. This work opens new pathways for future developments in accessible, cost-effective health monitoring, bridging research and clinical applications, with promising utility in clinical settings.

CRediT authorship contribution statement

Francesca Ceccardi: Writing – review & editing, Writing – original draft, Methodology, Investigation, Formal analysis. **Federica Mariani:** Writing – review & editing, Supervision, Project administration, Methodology, Investigation, Conceptualization. **Francesco Decataldo:** Writing – review & editing, Methodology, Investigation, Formal analysis, Conceptualization. **Vito Vurro:** Writing – review & editing, Formal analysis. **Marta Tessarolo:** Writing – review & editing, Project administration, Investigation, Funding acquisition, Conceptualization. **Isacco Gualandi:** Writing – review & editing, Supervision, Project administration, Methodology, Investigation, Funding acquisition, Conceptualization. **Beatrice Fraboni:** Writing – review & editing, Project administration, Funding acquisition, Conceptualization. **Erika Scavetta:** Writing – review & editing, Supervision, Project administration, Investigation, Funding acquisition, Conceptualization.

Declaration of competing interest

The authors declare the following financial interests/personal relationships which may be considered as potential competing interests:

Erika Scavetta reports financial support was provided by DSM Nutritional Products AG. If there are other authors, they declare that they have no known competing financial interests or personal relationships that could have appeared to influence the work reported in this paper.

Acknowledgments

The authors acknowledge DSM Nutritional Products for co-funding this project and for providing swine saliva samples essential to this research. We also extend our thanks to Elements srl for supplying the customized portable electronic equipment used in this study.

Supplementary materials

Supplementary material associated with this article can be found, in the online version, at doi:10.1016/j.electacta.2025.145834.

Data availability

Data will be made available on request.

References

[1] S. Jain, M. Nehra, R. Kumar, N. Dilbaghi, T.Y. Hu, S. Kumar, A. Kaushik, C. Zhong Li, Internet of medical things (IoMT)-integrated biosensors for point-of-care testing of infectious diseases, Biosens. Bioelectron. 179 (2021) 113074, https://doi.org/10.1016/j.bios.2021.113074.
[2] J.R. Choi, Development of point-of-care biosensors for COVID-19, Front. Chem. 8 (2020) 517, https://doi.org/10.3389/fchem.2020.00517.
[3] S.A. Soper, K. Brown, A. Ellington, B. Frazier, G. Garcia-Manero, V. Gau, S. I. Gutman, D.F. Hayes, B. Korte, J.L. Landers, D. Larson, F. Ligler, A. Majumdar, M. Mascini, D. Nolte, Z. Rosenzweig, J. Wang, D. Wilson, Point-of-care biosensor systems for cancer diagnostics/prognostics, Biosens. Bioelectron. 21 (2006) 1932–1942, https://doi.org/10.1016/j.bios.2006.01.006.
[4] J. Kim, A.S. Campbell, B.E.F. de Ávila, J. Wang, Wearable biosensors for healthcare monitoring, Nat. Biotechnol. 37 (2019) 389–406, https://doi.org/10.1038/s41587-019-0045-y.
[5] R.R. Nair, J.M. An, J. Kim, D. Kim, Review: recent progress in fluorescent molecular systems for the detection of disease-related biomarkers in biofluids, Coord. Chem. Rev. 494 (2023) 215336, https://doi.org/10.1016/j.ccr.2023.215336.
[6] Y. Bi, M. Sun, J. Wang, Z. Zhu, J. Bai, M.Y. Emran, A. Kotb, X. Bo, M. Zhou, Universal fully integrated wearable sensor arrays for the multiple electrolyte and metabolite monitoring in raw sweat, saliva, or urine, Anal. Chem. 95 (2023) 6690–6699, https://doi.org/10.1021/acs.analchem.3c00361.
[7] M. Gyurászová, R. Gurecká, J. Bábíčková, Ľ. Tóthová, Oxidative stress in the pathophysiology of kidney disease: implications for noninvasive monitoring and identification of biomarkers, Oxid. Med. Cell Longev. 2020 (2020) 5478708, https://doi.org/10.1155/2020/5478708.
[8] A.M. Pisoschi, A. Pop, The role of antioxidants in the chemistry of oxidative stress: a review, Eur. J. Med. Chem. 97 (2015) 55–74, https://doi.org/10.1016/j.ejmech.2015.04.040.
[9] R. Stocker, J.F. Keaney, Role of oxidative modifications in atherosclerosis, Physiol. Rev. 84 (2004) 1381–1478, https://doi.org/10.1152/physrev.00047.2003.
[10] A. Ghiselli, M. Serafini, F. Natella, C. Scaccini, Total antioxidant capacity as a tool to assess redox status: critical view and experimental data, Free Radic. Biol. Med. 29 (2000) 1106–1114, https://doi.org/10.1016/S0891-5849(00)00394-4.
[11] V. Lobo, A. Patil, A. Phatak, N. Chandra, Free radicals, antioxidants and functional foods: impact on human health, Pharmacogn. Rev. 4 (2010) 118–126, https://doi.org/10.4103/0973-7847.70902.
[12] O. Erel, A novel automated direct measurement method for total antioxidant capacity using a new generation, more stable ABTS radical cation, Clin. Biochem. 37 (2004) 277–285, https://doi.org/10.1016/j.clinbiochem.2003.11.015.
[13] C.P. Rubio, E. Mainau, J.J. Cerón, M.D. Contreras-Aguilar, S. Martínez-Subiela, E. Navarro, F. Tecles, X. Manteca, D. Escribano, Biomarkers of oxidative stress in saliva in pigs: analytical validation and changes in lactation, BMC Vet. Res. 15 (2019) 144, https://doi.org/10.1186/s12917-019-1875-z.
[14] D. Koracevic, G. Koracevic, V. Djordjevic, S. Andrejevic, V. Cosic, Method for the measurement of antioxidant activity in human fluids, J. Clin. Pathol. 54 (2001) 356–361, https://doi.org/10.1136/jcp.54.5.356.
[15] I. Peluso, A. Raguzzini, Salivary and urinary total antioxidant capacity as biomarkers of oxidative stress in humans, Patholog. Res. Int. 2016 (2016) 5480267, https://doi.org/10.1155/2016/5480267.
[16] A. Yaacob, N.H. Ngajikin, N.C.A. Rashid, M. Yaacob, S.H.A. Ali, N.E. Azmi, N. A. Cholan, Linearity range enhancement in direct detection of low concentration uric acid, Optik 249 (2022) 168243, https://doi.org/10.1016/j.ijleo.2021.168243.

[17] F. Mateos Anton, J.G. Puig, T. Ramos, P. Gonzilez, J. Ordris, Sex differences in uric acid metabolism in adults: evidence for a lack of influence of estradiol-17β (E_2) on the renal handling of urate, Metabolism. 35 (1986) 343–348, https://doi.org/10.1016/0026-0495(86)90152-6.

[18] N.E. Azmi, A.H.A. Rashid, J. Abdullah, N.A. Yusof, H. Sidek, Fluorescence biosensor based on encapsulated quantum dots/enzymes/sol-gel for non-invasive detection of uric acid, J. Lumin. 202 (2018) 309–315, https://doi.org/10.1016/j.jlumin.2018.05.075.

[19] N.E. Azmi, N.I. Ramli, J. Abdullah, M.A. Abdul Hamid, H. Sidek, S. Abd Rahman, N. Ariffin, N.A. Yusof, A simple and sensitive fluorescence based biosensor for the determination of uric acid using H_2O_2-sensitive quantum dots/dual enzymes, Biosens. Bioelectron. 67 (2015) 129–133, https://doi.org/10.1016/j.bios.2014.07.056.

[20] W. Pormsila, S. Krähenbühl, P.C. Hauser, Capillary electrophoresis with contactless conductivity detection for uric acid determination in biological fluids, Anal. Chim. Acta 636 (2009) 224–228, https://doi.org/10.1016/j.aca.2009.02.012.

[21] X. Peng, X. Li, B. Xie, Y. Lai, A. Sosnik, H. Boucetta, Z. Chen, W. He, Gout therapeutics and drug delivery, J. Controlled Release 362 (2023) 728–754, https://doi.org/10.1016/j.jconrel.2023.09.011.

[22] G. Ndrepepa, Uric acid and cardiovascular disease, Clin. Chim. Acta 484 (2018) 150–163, https://doi.org/10.1016/j.cca.2018.05.046.

[23] S. Wen, H. Arakawa, I. Tamai, Uric acid in health and disease: from physiological functions to pathogenic mechanisms, Pharmacol. Ther. 256 (2014) 108615, https://doi.org/10.1016/j.pharmthera.2024.108615.

[24] R. Ae, M. Kanbay, M. Kuwabara, The causality between the serum uric acid level and stroke, Hypertens. Res. 43 (2020) 354–356, https://doi.org/10.1038/s41440-019-0346-z.

[25] J. Perelló, P. Sanchis, F. Grases, Determination of uric acid in urine, saliva and calcium oxalate renal calculi by high-performance liquid chromatography/mass spectrometry, J. Chromatogr. B Anal. Technol. Biomed. Life Sci. 824 (2005) 175–180, https://doi.org/10.1016/j.jchromb.2005.07.024.

[26] Q. Wang, X. Wen, J. Kong, Recent progress on uric acid detection: a review, Crit. Rev. Anal. Chem. 50 (2020) 359–375, https://doi.org/10.1080/10408347.2019.1637711.

[27] N.J. Trengove, S.R. Langton, M.C. Stacey, Biochemical analysis of wound fluid from nonhealing and healing chronic leg ulcers, Wound Repair. Regen. 4 (1996) 234–239, https://doi.org/10.1046/j.1524-475X.1996.40211.x.

[28] Y.Y. al-Tamer 1, E.A. Hadi, I.I. al-Badrani, Sweat urea, uric acid and creatinine concentrations in uraemic patients, Urol. Res. 25 (1997) 337–340, https://doi.org/10.1007/BF01294662.

[29] K. Inoue, T. Namiki, Y. Iwasaki, Y. Yoshimura, H. Nakazawa, Determination of uric acid in human saliva by high-performance liquid chromatography with amperometric electrochemical detection, J. Chromatogr. B 785 (2003) 57–63, https://doi.org/10.1016/S1570-0232(02)00850-4.

[30] N.N. Rehak, S.A. Cecco, G. Csako, Biochemical composition and electrolyte balance of "unstimulated" whole human saliva, Clin. Chem. Lab. Med. 38 (2000) 335–343, https://doi.org/10.1515/CCLM.2000.049.

[31] A. Vernerová, L.K. Krčmová, O. Heneberk, V. Radochová, O. Strouhal, A. Kašparovský, B. Melichar, F. Švec, Chromatographic method for the determination of inflammatory biomarkers and uric acid in human saliva, Talanta 233 (2021) 797–812, https://doi.org/10.1016/j.talanta.2021.122598.

[32] S.H. Han, Y.J. Ha, E.H. Kang, K. Shin, Y.J. Lee, G.J. Lee, Electrochemical detection of uric acid in undiluted human saliva using uricase paper integrated electrodes, Sci. Rep. 12 (2022) 12033, https://doi.org/10.1038/s41598-022-16176-5.

[33] S.H. Han, K.W. Moon, Y.J. Lee, G.J. Lee, Simultaneous electrochemical analysis of uric acid and xanthine in human saliva and serum samples using a 3D reduced graphene oxide nanocomposite-modified electrode, Chemosensors 11 (2023) 185, https://doi.org/10.3390/chemosensors11030185.

[34] A. Vernerová, L. Kujovská Krčmová, B. Melichar, F. Švec, Non-invasive determination of uric acid in human saliva in the diagnosis of serious disorders, Clin. Chem. Lab. Med. 59 (2021) 797–812, https://doi.org/10.1515/cclm-2020-1533.

[35] J. Piedras, R.B. Dominguez, J.M. Gutiérrez, Determination of uric acid in artificial saliva with compact AMP3291 reader and au nanoparticles modified electrode, Chemosensors 9 (2021) 73, https://doi.org/10.3390/chemosensors9040073.

[36] G. Turkkan, S.Z. Bas, K. Atacan, M. Ozmen, An electrochemical sensor based on a Co_3O_4-ERGO nanocomposite modified screen-printed electrode for detection of uric acid in artificial saliva, Anal. Methods 14 (2022) 67–75, https://doi.org/10.1039/d1ay01744f.

[37] L. Bai, C.G. Elósegui, W. Li, P. Yu, J. Fei, L. Mao, Biological applications of organic electrochemical transistors: electrochemical biosensors and electrophysiology recording, Front. Chem. 7 (2019) 313, https://doi.org/10.3389/fchem.2019.00313.

[38] S.A. Wring, J.P. Hart, Chemically modified, carbon-based electrodes and their application as electrochemical sensors for the analysis of biologically important compounds a review, Analyst 117 (1992) 1215–1229, https://doi.org/10.1039/AN9921701215.

[39] J.M. Zen, A.S. Kumar, D.M. Tsai, Recent updates of chemically modified electrodes in analytical chemistry, Electroanalysis 15 (2003) 1073–1087, https://doi.org/10.1002/elan.200390130.

[40] P. Lin, F. Yan, Organic thin-film transistors for chemical and biological sensing, Adv. Mater. 24 (2012) 34–51, https://doi.org/10.1002/adma.201103334.

[41] T. Cramer, A. Campana, F. Leonardi, S. Casalini, A. Kyndiah, M. Murgia, F. Biscarini, Water-gated organic field effect transistors-opportunities for biochemical sensing and extracellular signal transduction, J. Mater. Chem. B 1 (2013) 3728–3741, https://doi.org/10.1039/c3tb20340a.

[42] A.V. Marquez, N. McEvoy, A. Pakdel, Organic electrochemical transistors (OECTs) toward flexible and wearable bioelectronics, Molecules 25 (2020) 5288, https://doi.org/10.3390/molecules25225288.

[43] D. Ohayon, V. Druet, S. Inal, A guide for the characterization of organic electrochemical transistors and channel materials, Chem. Soc. Rev. 52 (2023) 1001–1023, https://doi.org/10.1039/d2cs00920j.

[44] B. Piro, G. Mattana, S. Zrig, G. Anquetin, N. Battaglini, D. Capitao, A. Maurin, S. Reisberg, Fabrication and use of organic electrochemical transistors for sensing of metabolites in aqueous media, Appl. Sci. 8 (2018) 928, https://doi.org/10.3390/app8060928.

[45] M. Massetti, S. Zhang, P.C. Harikesh, B. Burtscher, C. Diacci, D.T. Simon, X. Liu, M. Fahlman, D. Tu, M. Berggren, S. Fabiano, Fully 3D-printed organic electrochemical transistors, Npj Flexible Electron. 7 (2023) 11, https://doi.org/10.1038/s41528-023-00245-4.

[46] D. Tu, S. Fabiano, Mixed ion-electron transport in organic electrochemical transistors, Appl. Phys. Lett. 117 (2020) 080501, https://doi.org/10.1063/5.0012599.

[47] S.T.M. Tan, S. Keene, A. Giovannitti, A. Melianas, M. Moser, I. McCulloch, A. Salleo, Operation mechanism of organic electrochemical transistors as redox chemical transducers, J. Mater. Chem. C. Mater. 9 (2021) 12148–12158, https://doi.org/10.1039/d1tc02224e.

[48] I. Gualandi, M. Marzocchi, E. Scavetta, M. Calienni, A. Bonfiglio, B. Fraboni, A simple all-PEDOT:PSS electrochemical transistor for ascorbic acid sensing, J. Mater. Chem. B 3 (2015) 6753–6762, https://doi.org/10.1039/c5tb00916b.

[49] I. Gualandi, D. Tonelli, F. Mariani, E. Scavetta, M. Marzocchi, B. Fraboni, Selective detection of dopamine with an all PEDOT:PSS organic electrochemical transistor, Sci. Rep. 6 (2016) 35419, https://doi.org/10.1038/srep35419.

[50] F. Bonafè, F. Decataldo, I. Zironi, D. Remondini, T. Cramer, B. Fraboni, AC amplification gain in organic electrochemical transistors for impedance-based single cell sensors, Nat. Commun. 13 (2022) 5423, https://doi.org/10.1038/s41467-022-33094-2.

[51] I. Gualandi, M. Tessarolo, F. Mariani, D. Tonelli, B. Fraboni, E. Scavetta, Organic electrochemical transistors as versatile analytical potentiometric sensors, Front. Bioeng. Biotechnol. 7 (2019) 354, https://doi.org/10.3389/fbioe.2019.00354.

[52] M. Galliani, C. Diacci, M. Berto, M. Sensi, V. Beni, M. Berggren, M. Borsari, D. T. Simon, F. Biscarini, C.A. Bortolotti, Flexible printed organic electrochemical transistors for the detection of uric acid in artificial wound exudate, Adv. Mater. Interfaces 7 (2020) 2001218, https://doi.org/10.1002/admi.202001218.

[53] Y. Tao, Y. Wang, R. Zhu, Y. Chen, X. Liu, M. Li, L. Yang, Y. Wang, D. Wang, Fiber based organic electrochemical transistor integrated with molecularly imprinted membrane for uric acid detection, Talanta 238 (2022) 123055, https://doi.org/10.1016/j.talanta.2021.123055.

[54] P. Hao, R. Zhu, Y. Tao, W. Jiang, X. Liu, Y. Tan, Y. Wang, D. Wang, Dual-analyte sensing with a molecularly imprinted polymer based on enhancement-mode organic electrochemical transistors, ACS. Appl. Mater. Interfaces 15 (2023) 30567–30579, https://doi.org/10.1021/acsami.3c04786.

[55] C. Liao, C. Mak, M. Zhang, H.L.W. Chan, F. Yan, Flexible organic electrochemical transistors for highly selective enzyme biosensors and used for saliva testing, Adv. Mater. 27 (2015) 676–681, https://doi.org/10.1002/adma.201404378.

[56] X. Gao, L. Zu, X. Cai, C. Li, H. Lian, Y. Liu, X. Wang, X. Cui, High performance of supercapacitor from PEDOT:PSS electrode and redox iodide ion electrolyte, Nanomaterials 8 (2018) 335, https://doi.org/10.3390/nano8050335.

[57] H.S. Park, S.J. Ko, J.S. Park, J.Y. Kim, H.K. Song, Redox-active charge carriers of conducting polymers as a tuner of conductivity and its potential window, Sci. Rep. 3 (2013) 2454, https://doi.org/10.1038/srep02454.

[58] R.N. Goyal, A. Brajter-Toth, G. Dryhurst, N.T. Nguyen, A comparison of the peroxidase-catalyzed and electrochemical oxidation of uric acid, Bioelectrochem. Bioenerg. 9 (1982) 39–60, https://doi.org/10.1016/0302-4598(82)80005-6.

[59] D. Arcangeli, I. Gualandi, F. Mariani, M. Tessarolo, F. Ceccardi, F. Decataldo, F. Melandri, D. Tonelli, B. Fraboni, E. Scavetta, Smart bandaid integrated with fully textile OECT for uric acid real-time monitoring in wound exudate, ACS Sens. 8 (2023) 1593–1608. https://doi.org/10.1021/acssensors.2c02728.

[60] F. Decataldo, I. Gualandi, M. Tessarolo, E. Scavetta, B. Fraboni, Transient-doped organic electrochemical transistors working in current-enhancing mode as sensing devices for low concentration of oxygen dissolved in solution, APL Mater. 8 (2020) 091103, https://doi.org/10.1063/5.0015232.

[61] R.S.P. Malon, S. Sadir, M. Balakrishnan, E.P. Córcoles, Saliva-based biosensors: noninvasive monitoring tool for clinical diagnostics, BioMed Res. Int. 2014 (2014) 1–20, https://doi.org/10.1155/2014/962903.

[62] T. Di Giulio, E. Mazzotta, C. Malatesta, Molecularly imprinted polyscopoletin for the electrochemical detection of the chronic disease marker lysozyme, Biosensors (Basel) 11 (2021) 1–18, https://doi.org/10.3390/bios11010003.

[63] E. Tékus, M. Kaj, E. Szabó, N.L. Szénási, I. Kerepesi, M. Figler, R. Gábriel, M. Wilhelm, Comparison of blood and saliva lactate level after maximum intensity exercise, Acta. Biol. Hung. 63 (2012) 89–98, https://doi.org/10.1556/abiol.63.2012.suppl.1.9.

[64] S. Gupta, M.T. Nayak, J.D. Sunitha, G. Dawar, N. Sinha, N.S. Rallan, Correlation of salivary glucose level with blood glucose level in diabetes mellitus, J. Oral Maxillofac. Pathol. 21 (2017) 334–339, https://doi.org/10.4103/jomfp.JOMFP_222_15.

[65] S.K. Arya, G. Chornokur, M. Venugopalb, S. Bhansali, Antibody functionalized interdigitated μ-electrode (IDμE) based impedimetric cortisol biosensor, Analyst 135 (2010) 1941–1946, https://doi.org/10.1039/C0AN00242A.

[66] E. Mäkilä, P. Kirveskari, A study of ascorbic acid in human saliva, Arch. Oral Biol. 14 (1969) 1285–1292, https://doi.org/10.1016/0003-9969(69)90201-5.

[67] T. Okumura, Y. Nakajima, M. Matsuoka, T. Takamatsu, Study of salivary catecholamines using fully automated column switching high-performance liquid chromatography, J. Chromatogr. B Biomed. Sci. Appl. 694 (1997) 305–316, https://doi.org/10.1016/S0378-4347(97)00106-0.
[68] P. Żukowski, M. Maciejczyk, D. Waszkiel, Sources of free radicals and oxidative stress in the oral cavity, Arch. Oral Biol. 92 (2018) 8–17, https://doi.org/10.1016/j.archoralbio.2018.04.018.
[69] B. Čižmárová, V. Tomečková, B. Hubková, A. Hurajtová, J. Ohlasová, A. Birková, Salivary redox homeostasis in human health and disease, Int. J. Mol. Sci. 23 (2022) 10076, https://doi.org/10.3390/ijms231710076.
[70] H. Sies, D.P. Jones, Reactive oxygen species (ROS) as pleiotropic physiological signalling agents, Nat. Rev. Mol. Cell Biol. 21 (2020) 363–383, https://doi.org/10.1038/s41580-020-0230-3.
[71] A. Ramirez, C. Wang, J.R. Prickett, R. Pogranichniy, K.J. Yoon, R. Main, J. K. Johnson, C. Rademacher, M. Hoogland, P. Hoffmann, A. Kurtz, E. Kurtz, J. Zimmerman, Efficient surveillance of pig populations using oral fluids, Prev. Vet. Med. 104 (2012) 292–300, https://doi.org/10.1016/j.prevetmed.2011.11.008.
[72] M.J. López-Martínez, D. Escribano, A. Ortín-Bustillo, L. Franco-Martínez, L. G. González-Arostegui, J.J. Cerón, C.P. Rubio, Changes in biomarkers of redox status in saliva of pigs after an experimental sepsis induction, Antioxidants 11 (2022) 1380, https://doi.org/10.3390/antiox11071380.